Uncovering the geometry of the hot X-ray corona in the Seyfert galaxy NGC 4151

V. E. Gianolli and D. E. Kim
on behalf of the IXPE collaboration

Journées PNHE 2023
07/09/2023

IXPE:
from I, Q and U spectra to PD/PA

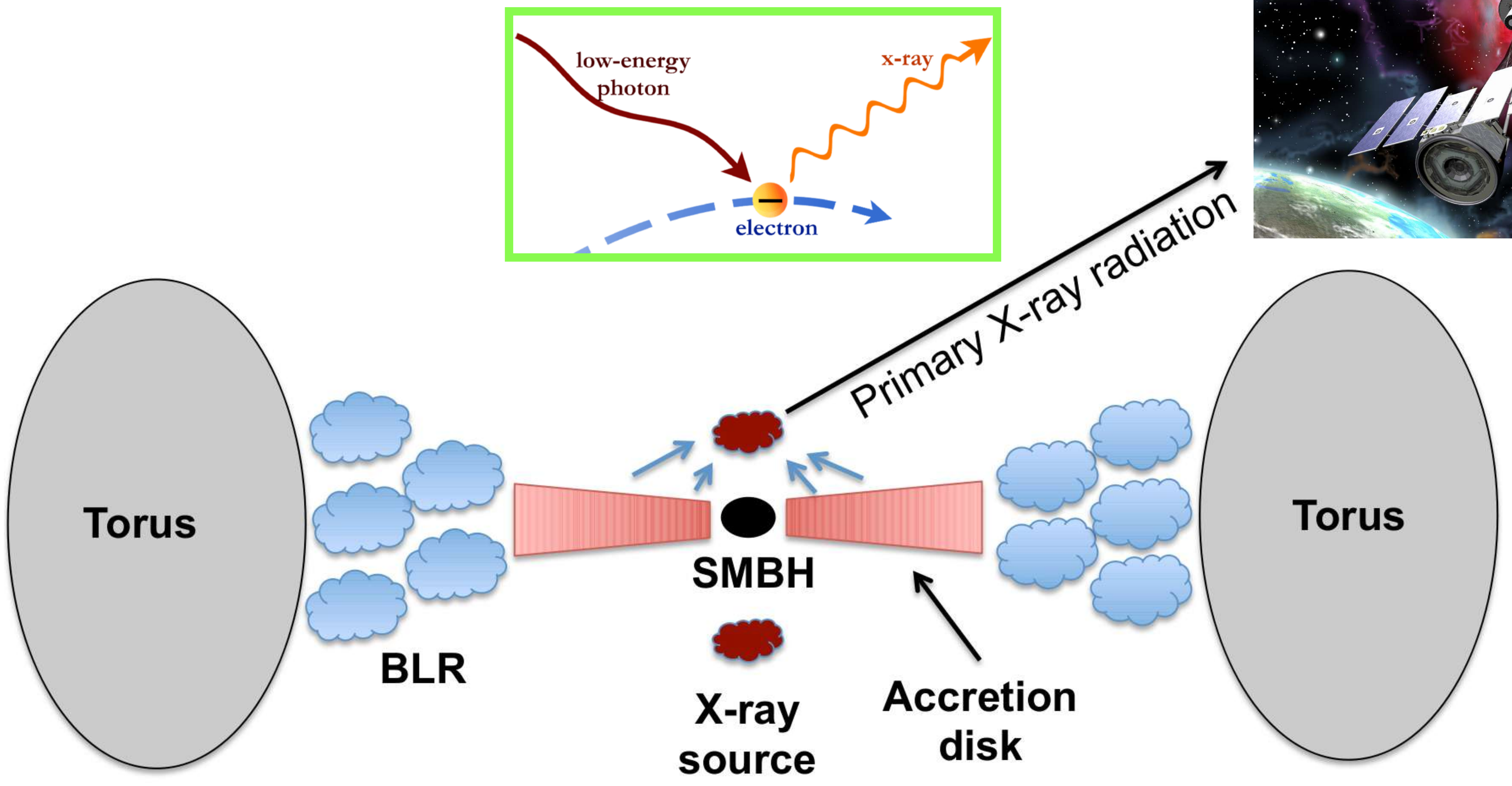

For more infos:
Bellazzini & Muleri, 2010

For each Detector Unit (DU) 3 spectra:

I = total intensity

Q = intensity linearly polarized at 90°

U = intensity linearly polarized at ± 45°

polarization information is encoded in the Stokes parameters:

I, Q and U

About the system:

symmetry ⟷ Polarization Degree $= \Pi = \dfrac{\sqrt{Q^2 + U^2}}{I}$

orientation ⟷ Polarization Angle $= \Psi = \dfrac{1}{2} arctg(\dfrac{U}{Q})$

IXPE
Imaging
X-Ray
Polarimetry
Explorer

Time for presentation…

- Changing Look AGN:

Antonucci & Cohen 1983; Penston & Perez 1984; Puccetti et al. 2007; Shapovalova et al. 2008, Shapovalova et al. 2012; Beuchert et al. 2017a

optical type 1.5* at high flux states (up to $F_{0.5-10\ \mathrm{keV}} \sim 2.8\times10^{-10}$ erg s^{-1} cm^{-2})

optical type 1.8† at low fluxes states ($F_{0.5-10\ \mathrm{keV}} \sim 8.7\times10^{-11}$ erg s^{-1} cm^{-2})

- z = 0.003326
- $M_{BH} \sim 4.6 \times 10^7\ M_\odot$ (from optical and UV reverberation, Bentz et al., 2006)
- $\lambda_{Edd} \sim 1\%$ Keck et al., 2015

* strong and variable optical-UV continuum with broad Hβ component and 1<[OIII]/Hβ<4
† strong and variable optical-UV continuum with weak broad Hβ component and 4<[OIII]/Hβ

Time for presentation…

- Complex absorption structure from neutral and ionised gas (Beuchert et al. 2017a)
- Strong Fe Kα emission line:

  In the past… with a weak relativistic component (Zoghbi et al. 2019)

  Now… single Gaussian with σ = 40±10 eV and EW = 100±6 eV
- Below 2 keV the soft X-ray emission is dominated by emission lines (NLR) (Schurch et al. 2004)
- Significant spectral variability above ~1 keV

X-ray polarization

uncertainties at 68% c.l.
contours at 68%, 90% and 99% c.l.

Energy range (keV)	$\Pi_X \pm 1\sigma$ (%)	$\psi_X \pm 1\sigma$ (deg)
2.0 – 8.0	4.9 ± 1.1	86 ± 7
2.0 – 3.5	4.3 ± 1.6	42 ± 11
3.5 – 5.0	5.0 ± 1.4	99 ± 8
5.0 – 8.0	7.4 ± 1.9	88 ± 7

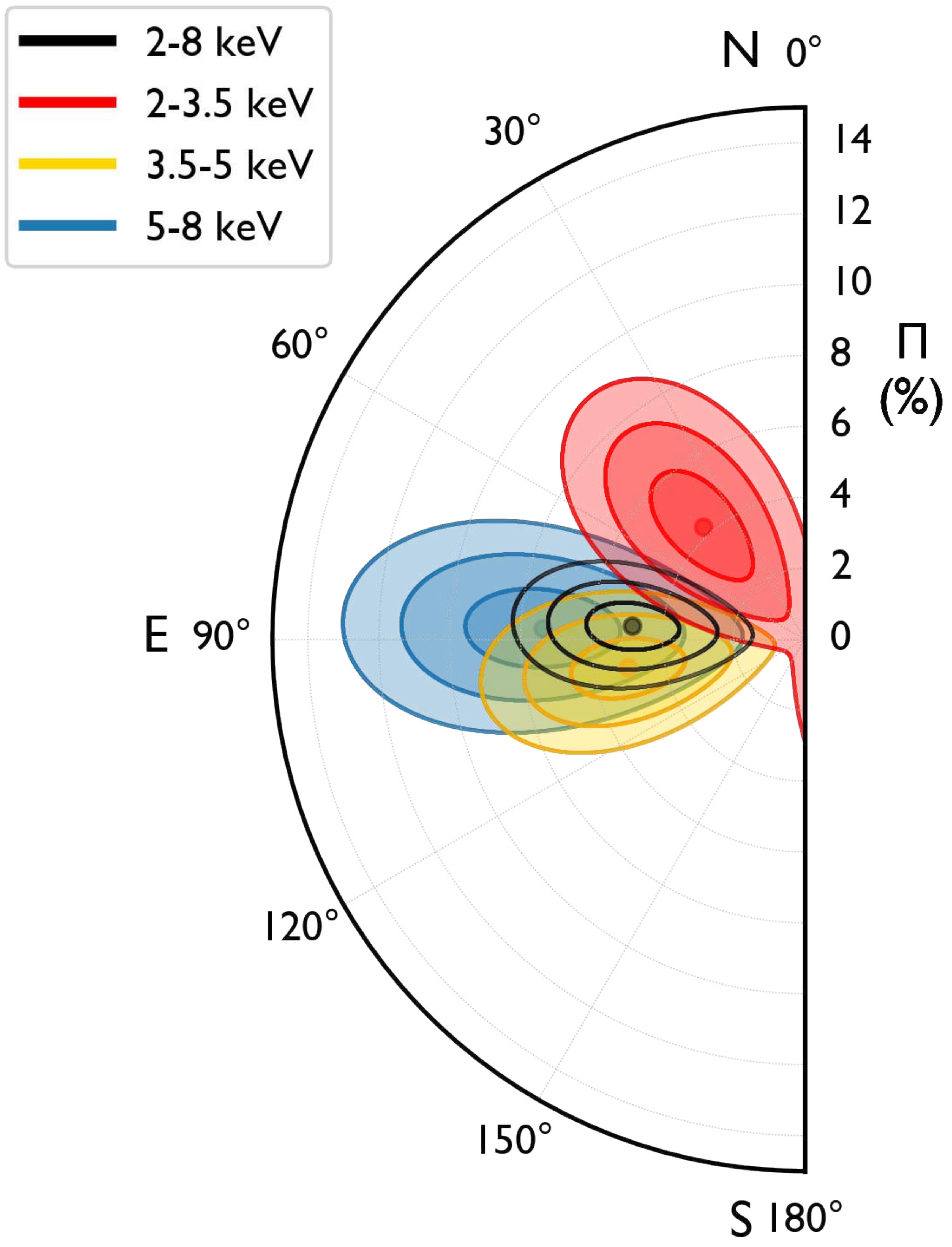

X-ray polarization

uncertainties at 68% c.l.
contours at 68%, 90% and 99% c.l.

Energy range (keV)	$\Pi_X \pm 1\sigma$ (%)	$\psi_X \pm 1\sigma$ (deg)
2.0 – 8.0	4.9 ± 1.1	86 ± 7
2.0 – 3.5	4.3 ± 1.6	42 ± 11
3.5 – 5.0	5.0 ± 1.4	99 ± 8
5.0 – 8.0	7.4 ± 1.9	88 ± 7

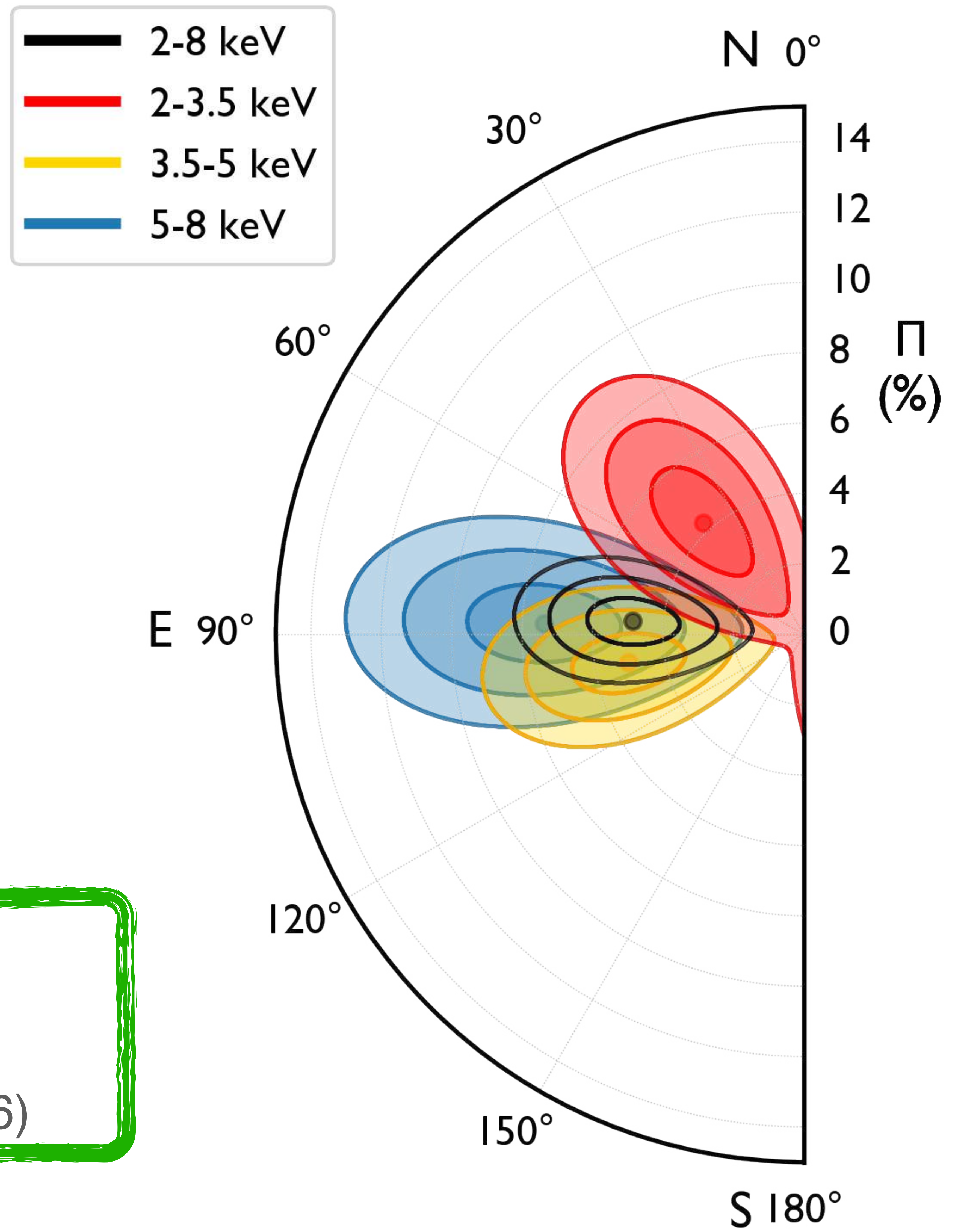

The obtained PA is well aligned with the one in UV, optical, NIR and nuclear radio jet, PA ~ 83°

(Harrison et al., 1986)

Model

Parameter	Value
CLOUDY (Photoionized emitter)	
$\log U$	1.35 ± 0.01
$\log(N_H / cm^{-2})$	21.63 ± 0.02
PC 1 (Neutral absorber 1)	
$\log(N_H / cm^{-2})$	10.49 ± 0.04
Cf	0.78 ± 0.01
PC 2 (Neutral absorber 2)	
$\log(N_H / cm^{-2})$	4.36 ± 0.01
Cf	0.95 ± 0.01
WA (Warm absorber)	
$\log(N_H / cm^{-2})$	$13.60^{+0.92}_{-0.86}$
$\log(\xi / erg\ cm\ s^{-1})$	4.12 ± 0.02
BORUS 1/2 (Neutral reflector 1/2)	
$\log(N_H / cm^{-2})$	24.45 ± 0.01
A_{Fe}	0.62 ± 0.01
norm	0.09 ± 0.01
nthcomp (Comptonized primary continuum)	
Γ	1.85 ± 0.01
kT_e [keV]	60^{+7}_{-6}
norm	0.09 ± 0.01
$\log(F_{2-10\ keV} / erg\ cm^{-2}\ s^{-1})$	-9.78 ± 0.01
$\log(L_{2-10\ keV} / erg\ s^{-1})$	42.61 ± 0.01

Implemented from Keck et al. 2015 and Szanecki et al. 2021 works

TBabs*(CLOUDY + zgauss + zpcfabs*zpcfabs*zxipcf

(gsmooth*(BORUS_c + BORUS_l) + nthComp))

On XMM+NuSTAR

χ^2/d.o.f = 743/660

Model

TBabs*(CLOUDY + zgauss + zpcfabs*zpcfabs*zxipcf (gsmooth*(BORUS_c + BORUS_l) + nthComp))

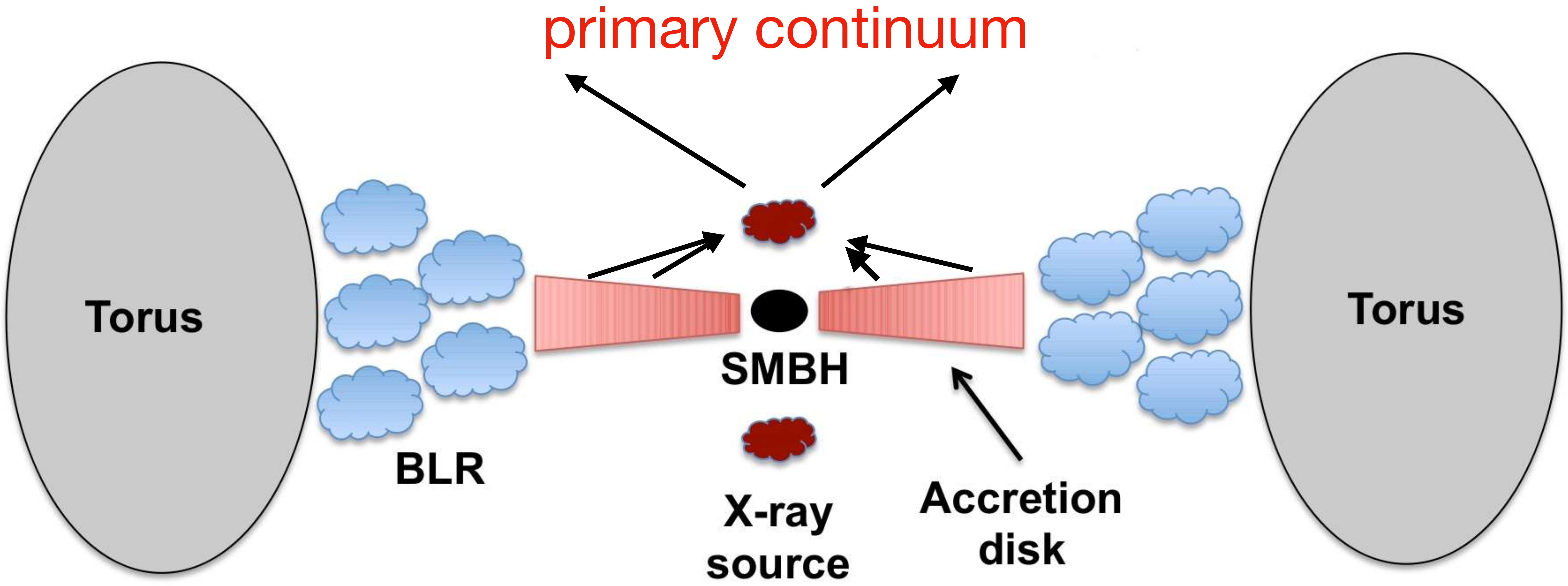

Model

TBabs*(CLOUDY + zgauss + zpcfabs*zpcfabs*zxipcf (gsmooth*(BORUS_c + BORUS_l) + nthComp))

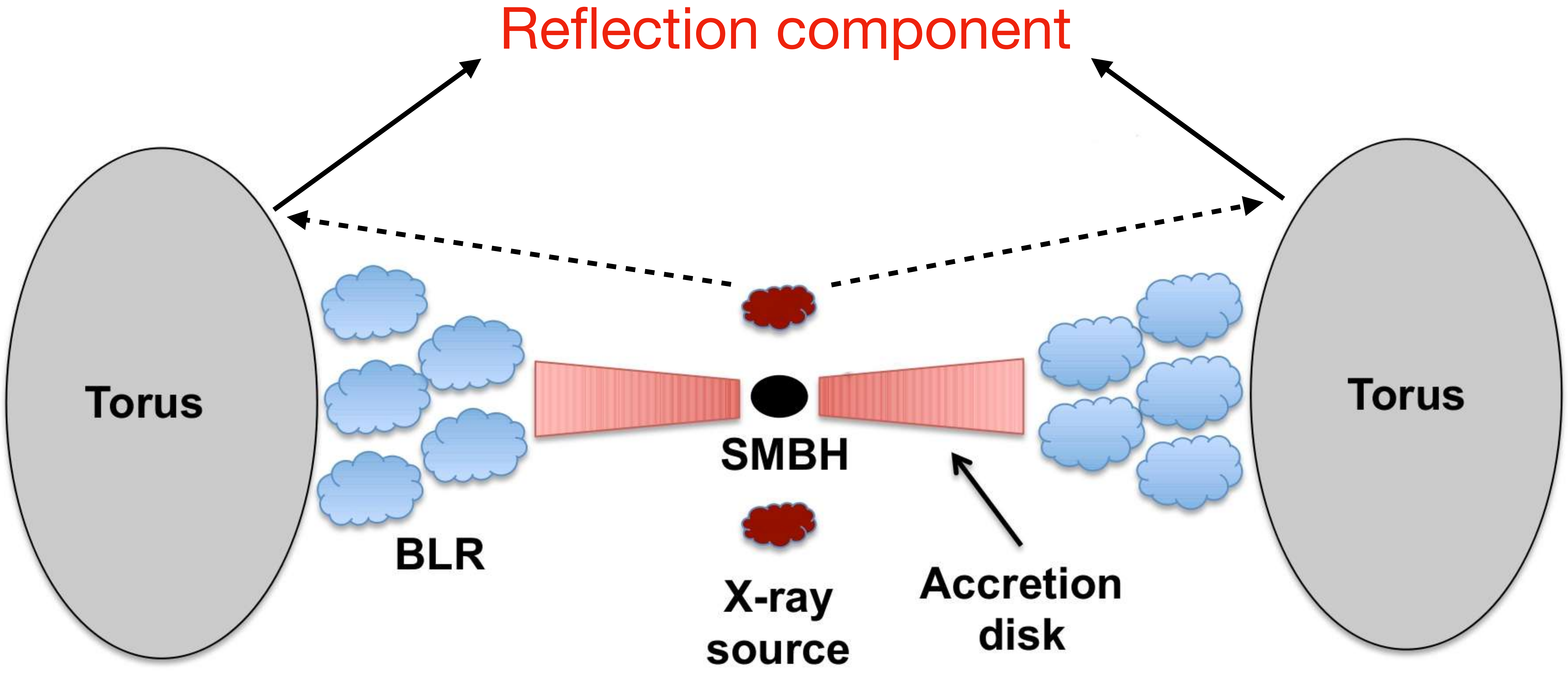

Model

TBabs*(CLOUDY + zgauss + zpcfabs*zpcfabs*zxipcf (gsmooth*(BORUS_c + BORUS_l) + nthComp))

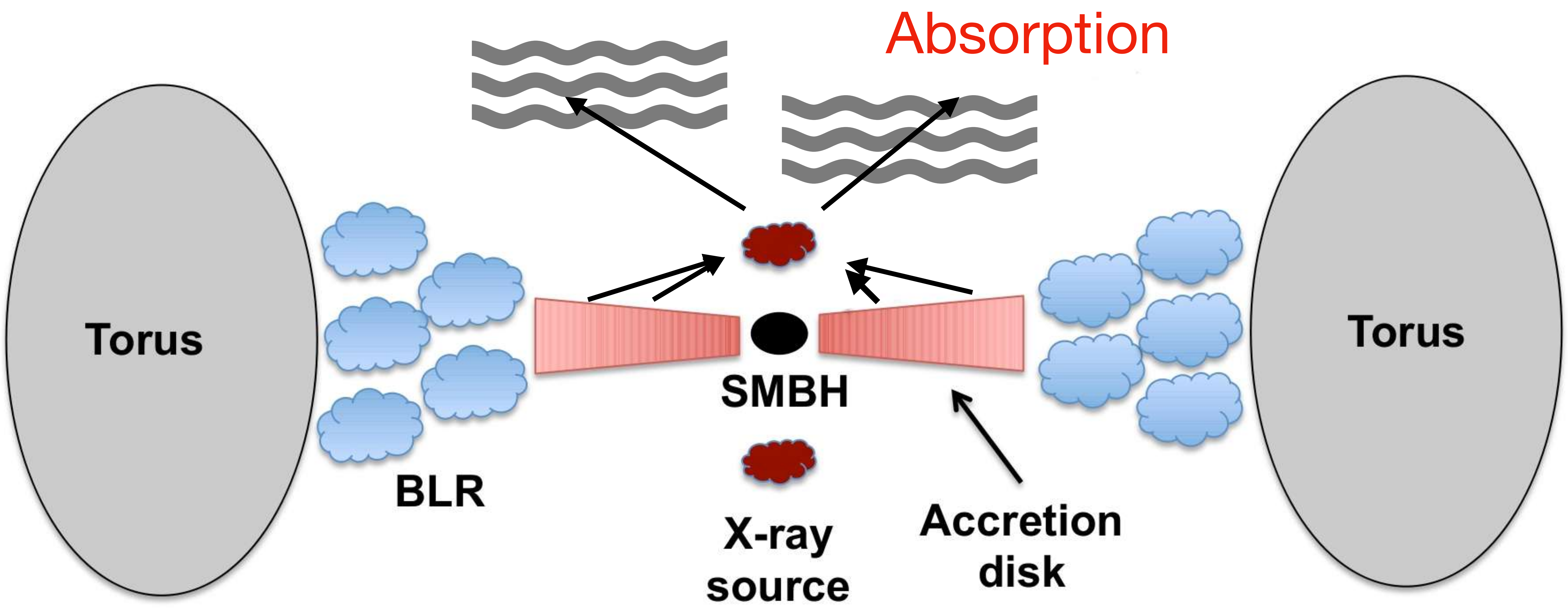

Model

TBabs*(CLOUDY + zgauss + zpcfabs*zpcfabs*zxipcf (gsmooth*(BORUS_c + BORUS_l) + nthComp))

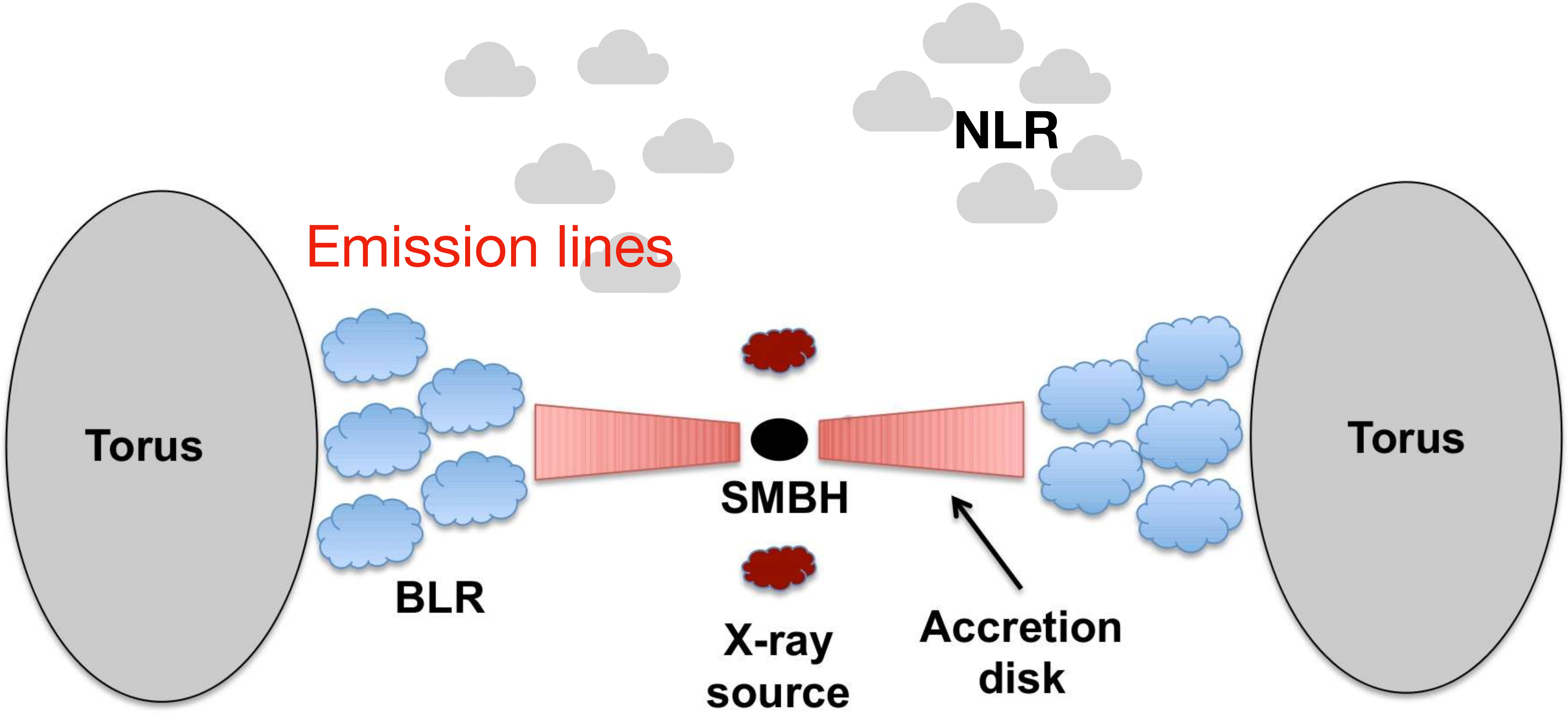

Model: polconst addition

TBabs*(CLOUDY + zgauss + zpcfabs*zpcfabs*zxipcf (gsmooth*(BORUS_c + BORUS_l) + nthComp))

PA = 0
PD = 0

XMM+NuSTAR+IXPE:

χ^2/d.o.f = 1433/1264

PA = 0
PD = 0

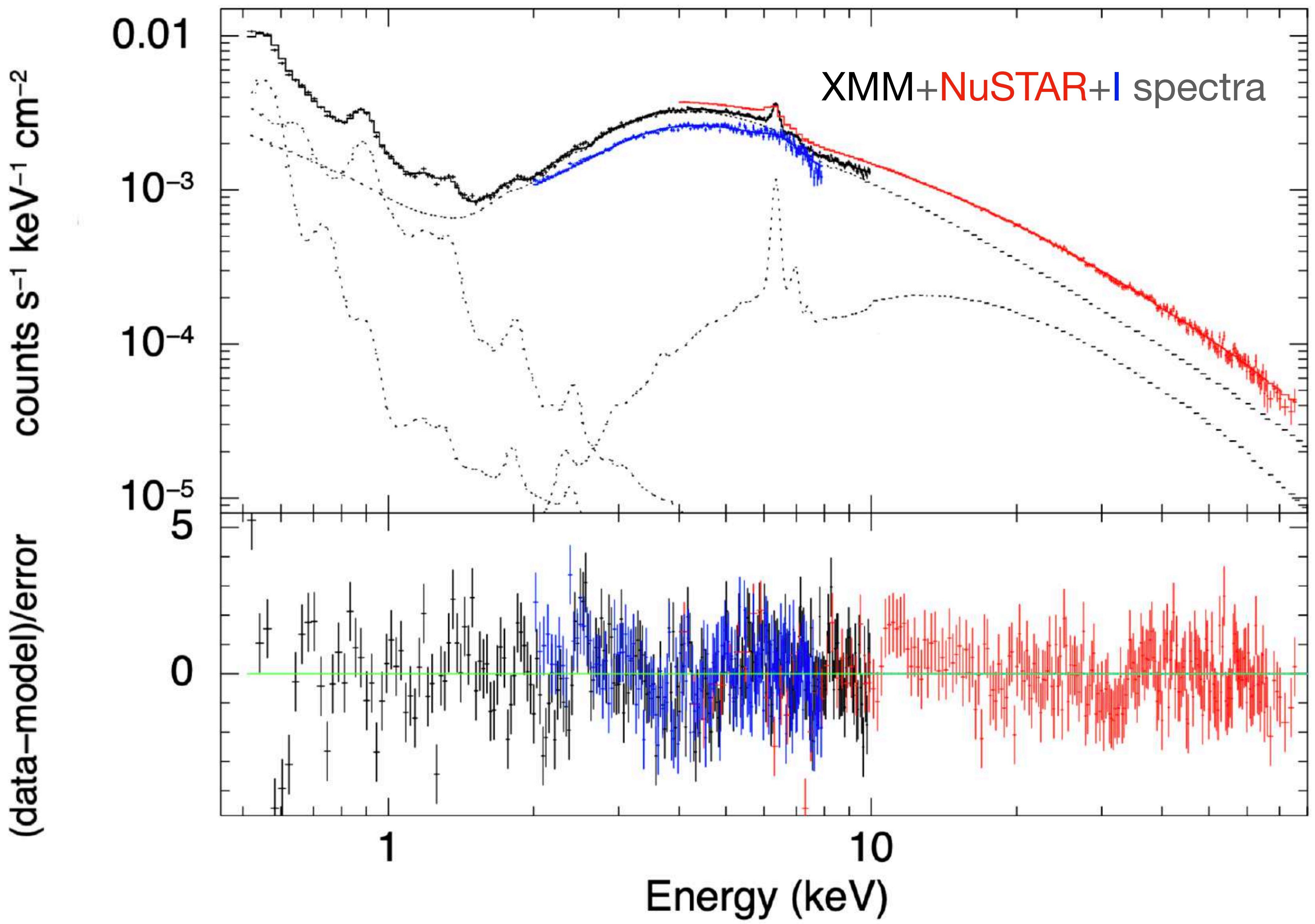

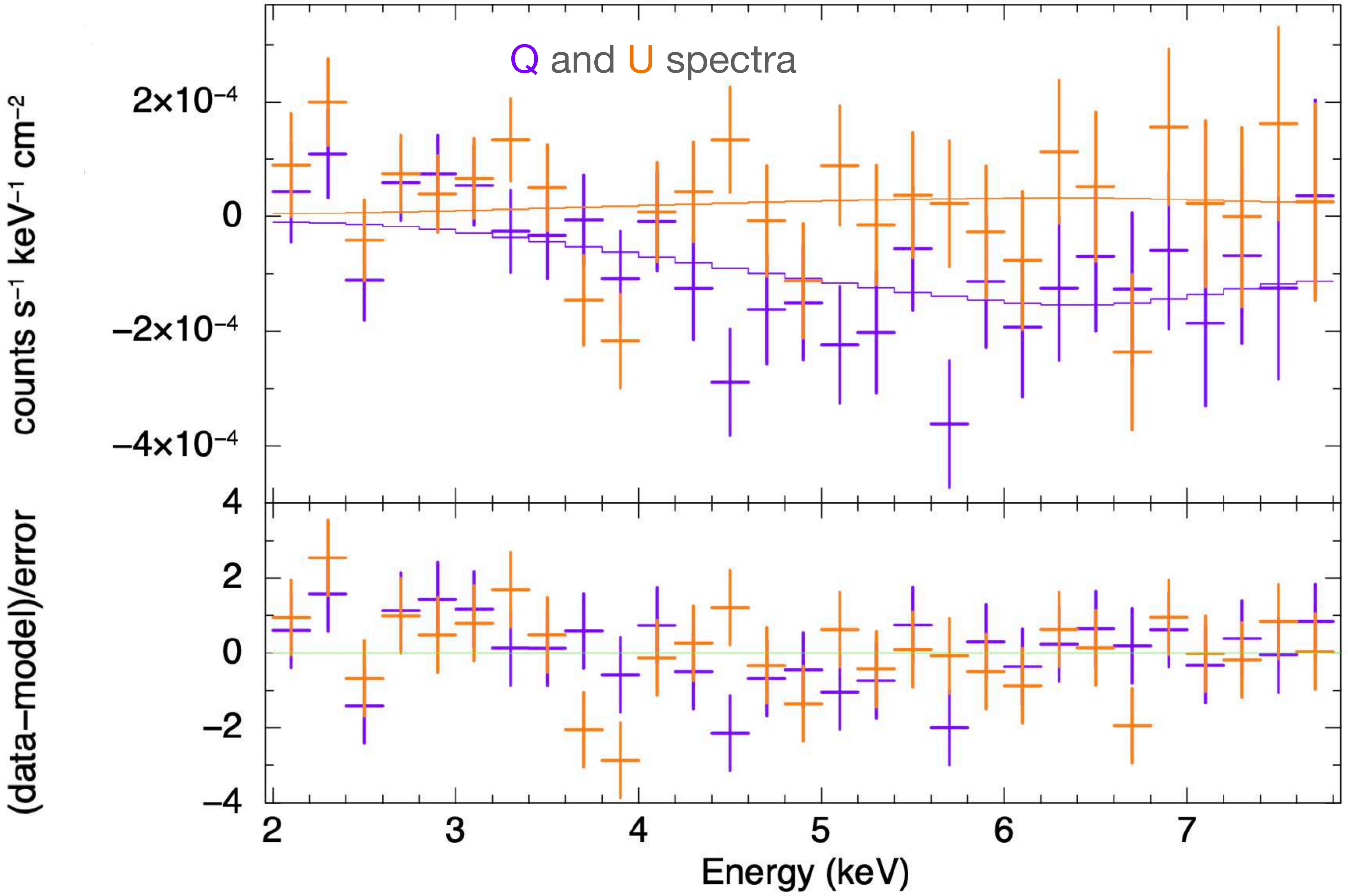

Spectro-polarimetric analysis

Primary:

$\Pi_P < 5\%$

unconstrained Ψ_P

Reflection:

$\Pi_R > 38\%$

$\Psi_R = 96 \pm 16°$

uncertainties at 68% c.l.
upper/lower limits at 99.7% c.l.

1st test: $\Psi_R = \Psi_P$ (χ^2/d.o.f = 1435/1265)

2nd test: Ψ_R and Ψ_P differ by 90° (χ^2/d.o.f = 1434/1265)

↓

polarization is dominated by the reflection and the PD of the primary emission is an upper limit

Spectro-polarimetric analysis

3rd test:

fixed values for Π_R
+
Ψ_R and Ψ_P differ by 90°

	15%	20%	30%
Π_P	4.1 ± 0.8 %	4.3 ± 0.8 %	4.6 ± 0.8 %
Ψ_P	82 ± 7 °	81 ± 7 °	80 ± 8 °
χ^2/d.o.f	1452/1266	1453/1266	1455/1266

Spectro-polarimetric analysis

To decouple the leaked soft X-ray emission from the primary emission

zpcfabs*(BORUS_c + BORUS_l + nthComp)

↓

(c*zphabs+(1-c))*(BORUS_c + BORUS_l + nthComp)

assign polconst ($\Pi = 0$ and $\Psi = 0$) to the leaked emission

Spectro-polarimetric analysis

zpcfabs*(BORUS_c + BORUS_l + nthComp)

↓

(c*zphabs+(1-c))*(BORUS_c + BORUS_l + nthComp)

$\Psi_R \neq \Psi_C$:
polarization is dominated by the reflection
(χ^2/d.o.f =1436/1264)

→

	$\Psi_R = \Psi_P$	$\Psi_R = \Psi_P \pm 90°$
Primary	$\Pi = 3 \pm 2$ % $\Psi = 88 \pm 5°$	$\Pi = 7.7 \pm 1.5$ % $\Psi = 87 \pm 6°$
Reflection	unconstrained Π	Π < 27%
χ^2/d.o.f	1437/1265	1441/1265

Spectro-polarimetric analysis

zpcfabs*(BORUS_c + BORUS_l + nthComp)

↓

(c*zphabs+(1-c))*(BORUS_c + BORUS_l + nthComp)

$\Psi_R \neq \Psi_C$:
polarization is dominated by the reflection
(χ^2/d.o.f =1436/1264)

	$\Psi_R = \Psi_P$	$\Psi_R = \Psi_P \pm 90°$
Primary	$\Pi = 3 \pm 2$ % $\Psi = 88 \pm 5°$	$\Pi = 7.7 \pm 1.5$ % $\Psi = 87 \pm 6°$
Reflection	unconstrained Π	$\Pi < 27\%$
χ^2/d.o.f	1437/1265	1441/1265

UV-OPT-IR Polarization

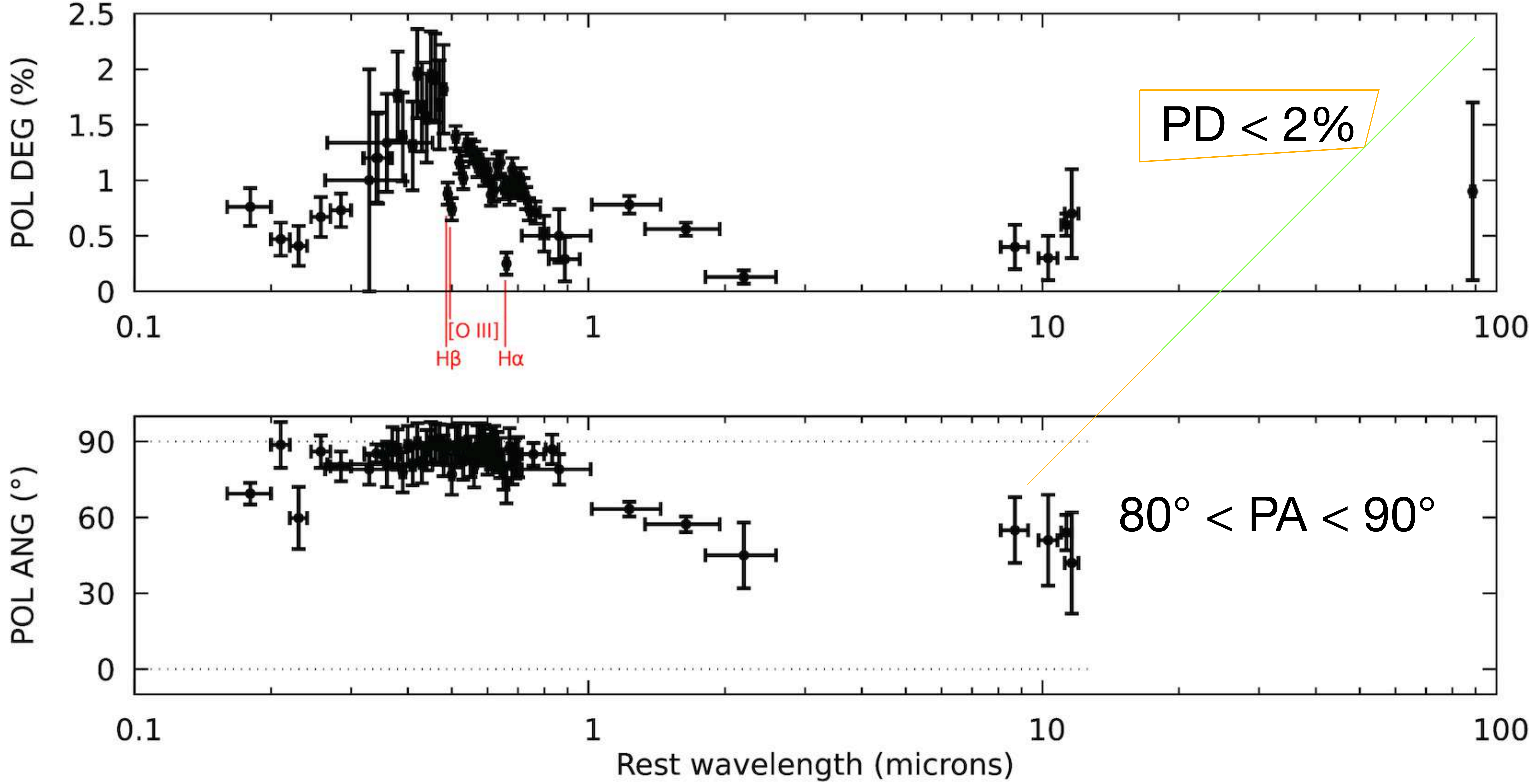

The X-ray PA is well aligned with the one in UV, optical, NIR and nuclear radio jet, PA ~ 83°
(Harrison et al., 1986)

Marin et al., 2020

Coronal geometry(ies)

'Spherical' lamppost geometry:

- spectro-polarimetric analysis

Π_P in the 4-8% range

- model-independent analysis (PCUBE)

$\Pi_X = 4.9 \pm 1.1\%$

- expected $\Psi \perp$ disc axis

Slab geometry:

$R_{\rm in} = R_{\rm ISCO} = 1.24 r_{\rm g}$

$R_{\rm out} = 100 r_{\rm g}$

Height = $1 r_{\rm g}$

Wedge geometry:

$R_{\rm in} = R_{\rm ISCO} = 1.24 r_{\rm g}$

$R_{\rm out} = R_{\rm in}^{\rm disk} = 25 r_{\rm g}$

α = 30°, 45°, 60°

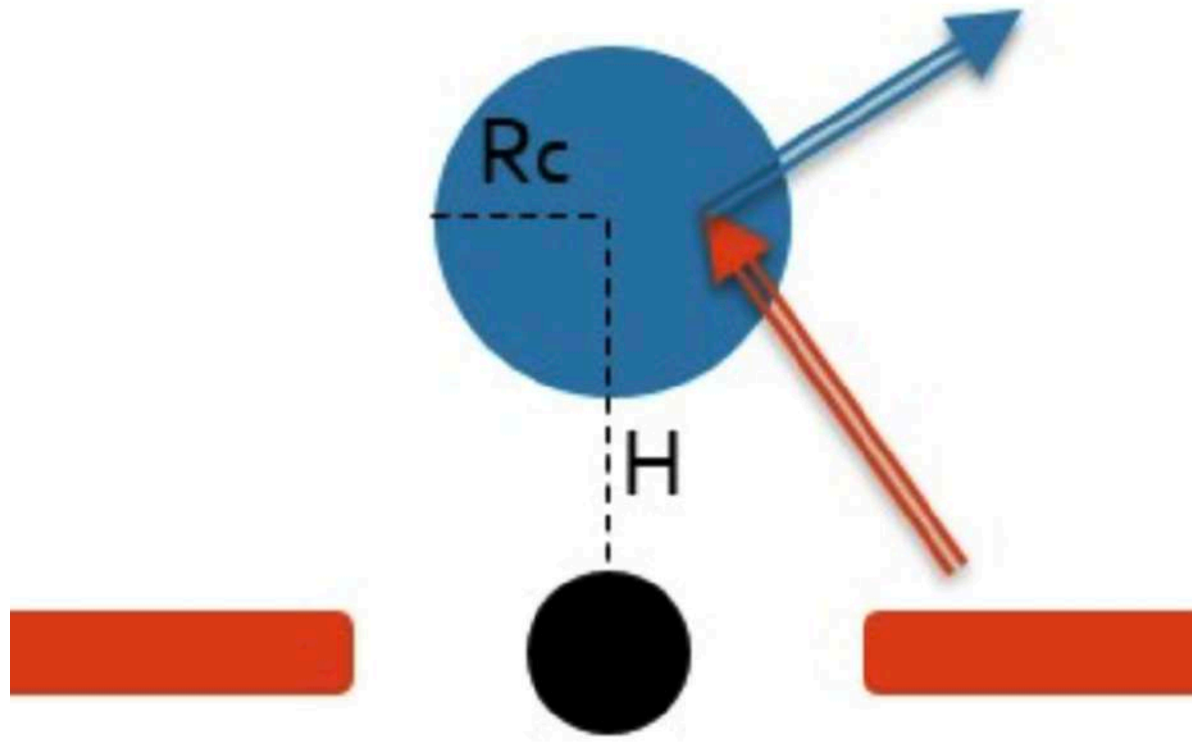

Ursini et al., 2022

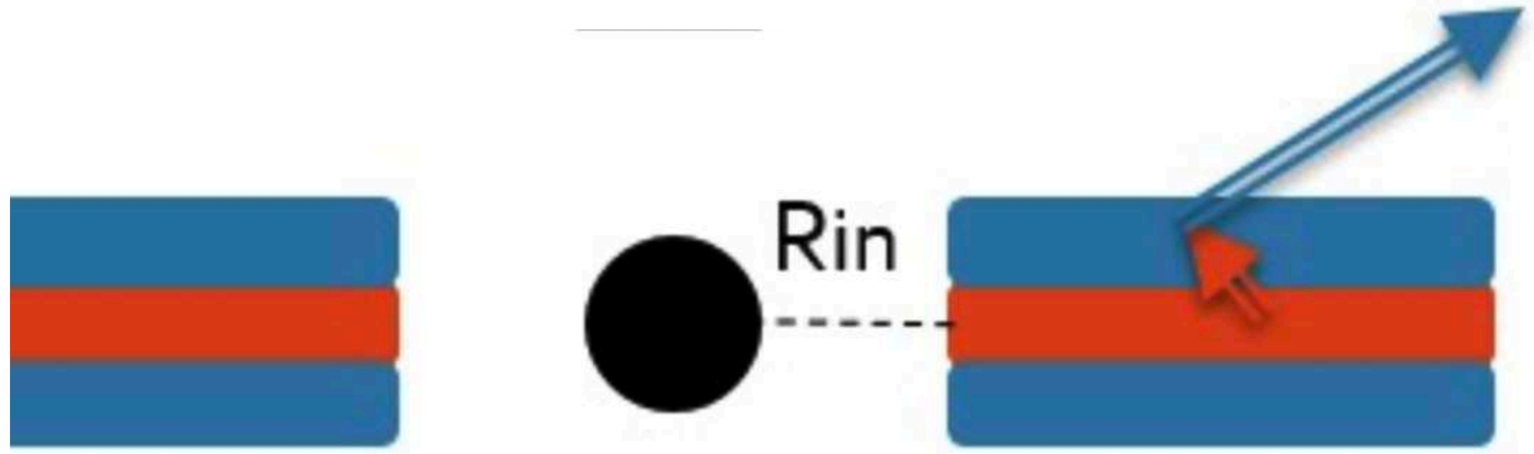

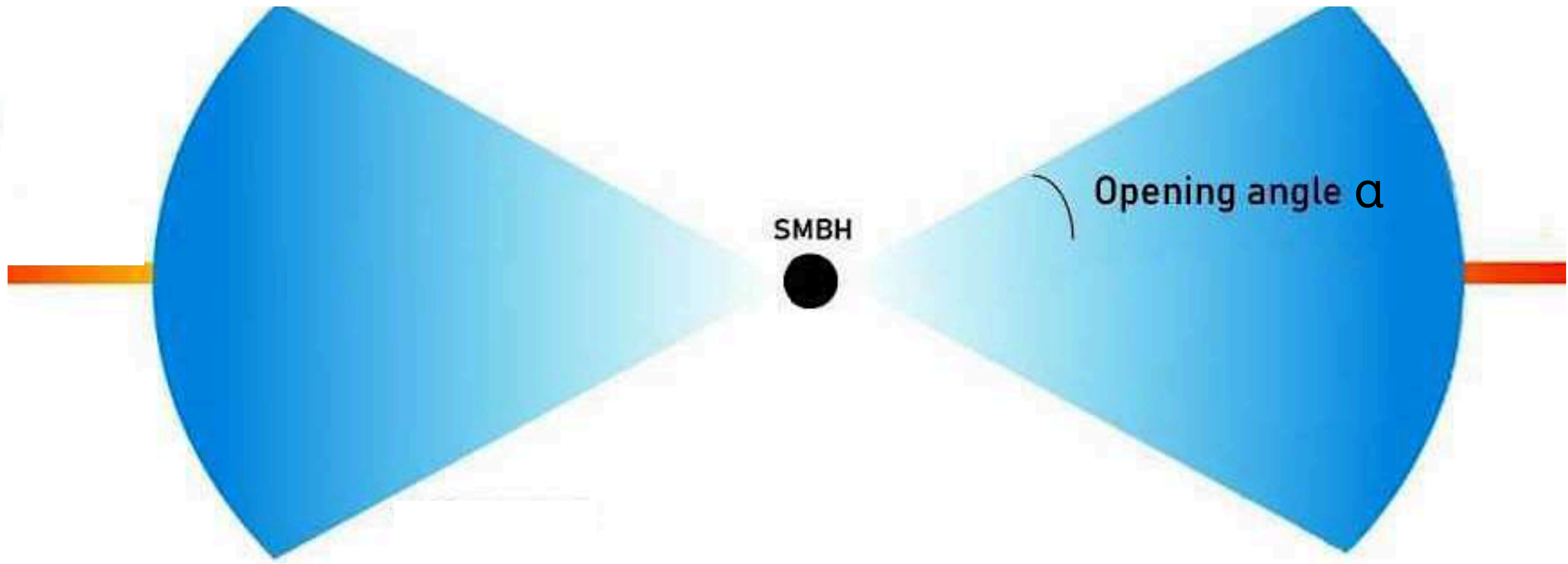

Tagliacozzo et al., subm.

Coronal geometry(ies)

‘Spherical’ lamppost geometry:

- spectro-polarimetric analysis

Π_P in the 4-8% range

- model-independent analysis (PCUBE)

$\Pi_X = 4.9 \pm 1.1\%$

- expected $\Psi \perp$ disc axis

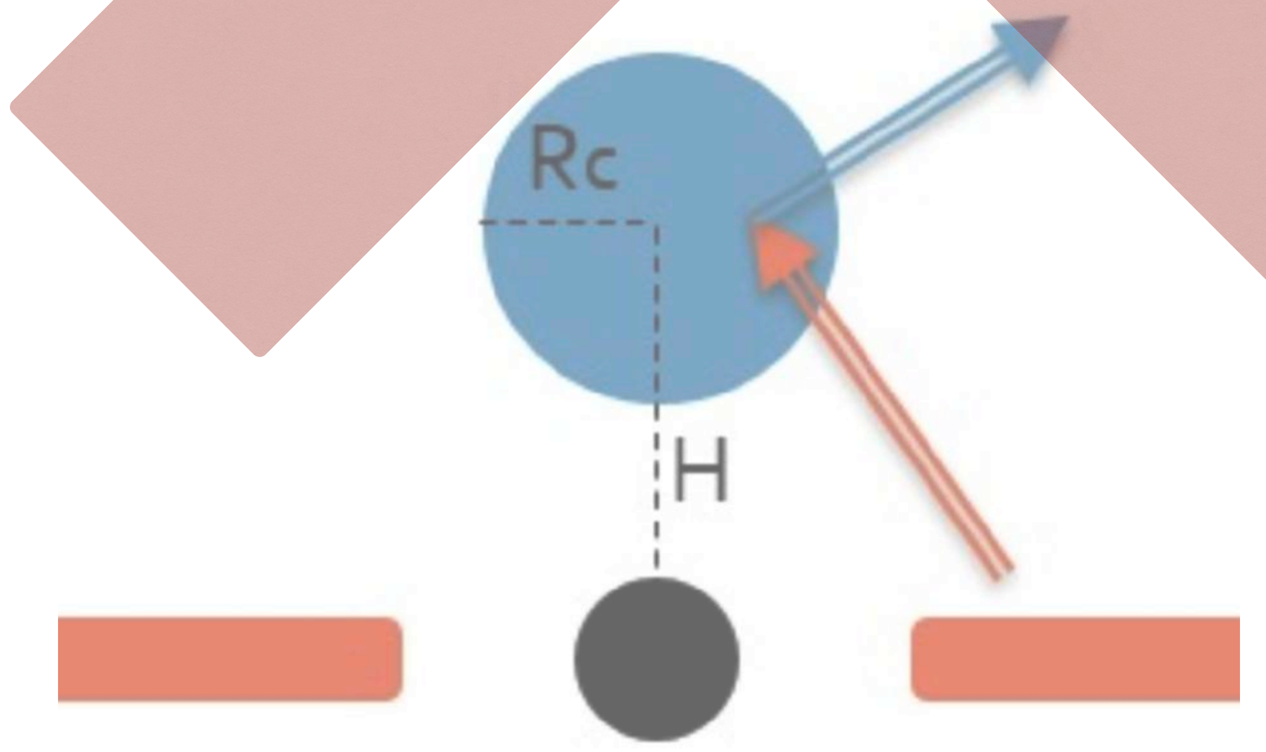

Ursini et al., 2022

Slab geometry:

$$R_{\rm in} = R_{\rm ISCO} = 1.24 r_g$$

$$R_{\rm out} = 100 r_g$$

$$\text{Height} = 1 r_g$$

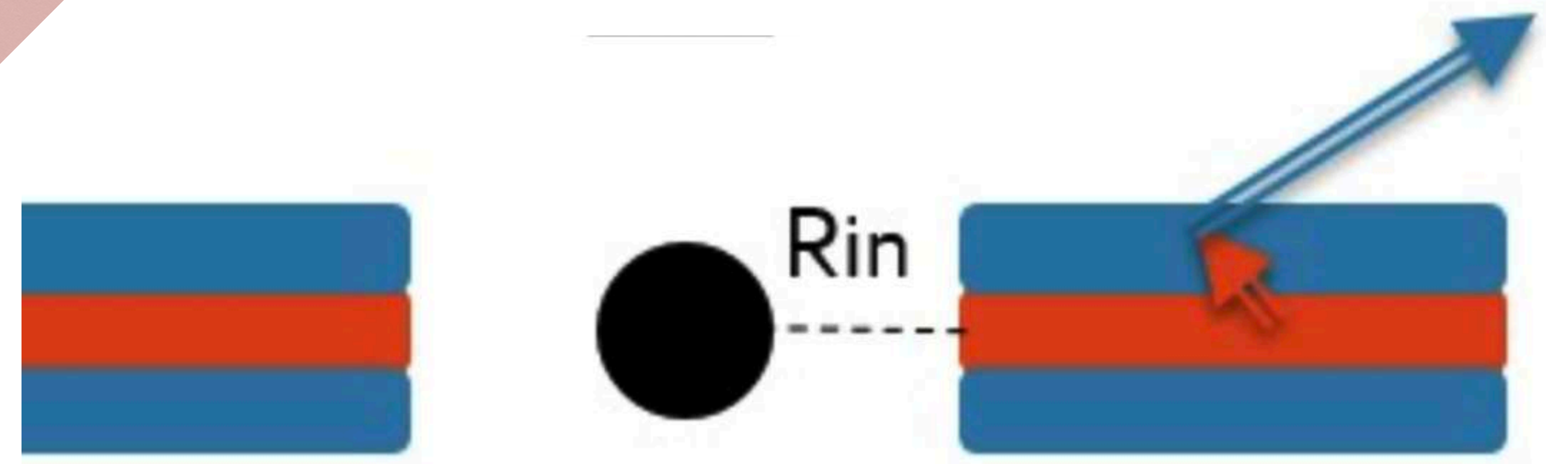

Wedge geometry:

$$R_{\rm in} = R_{\rm ISCO} = 1.24 r_g$$

$$R_{\rm out} = R_{\rm in}^{\rm disk} = 25 r_g$$

$\alpha = 30°, 45°, 60°$

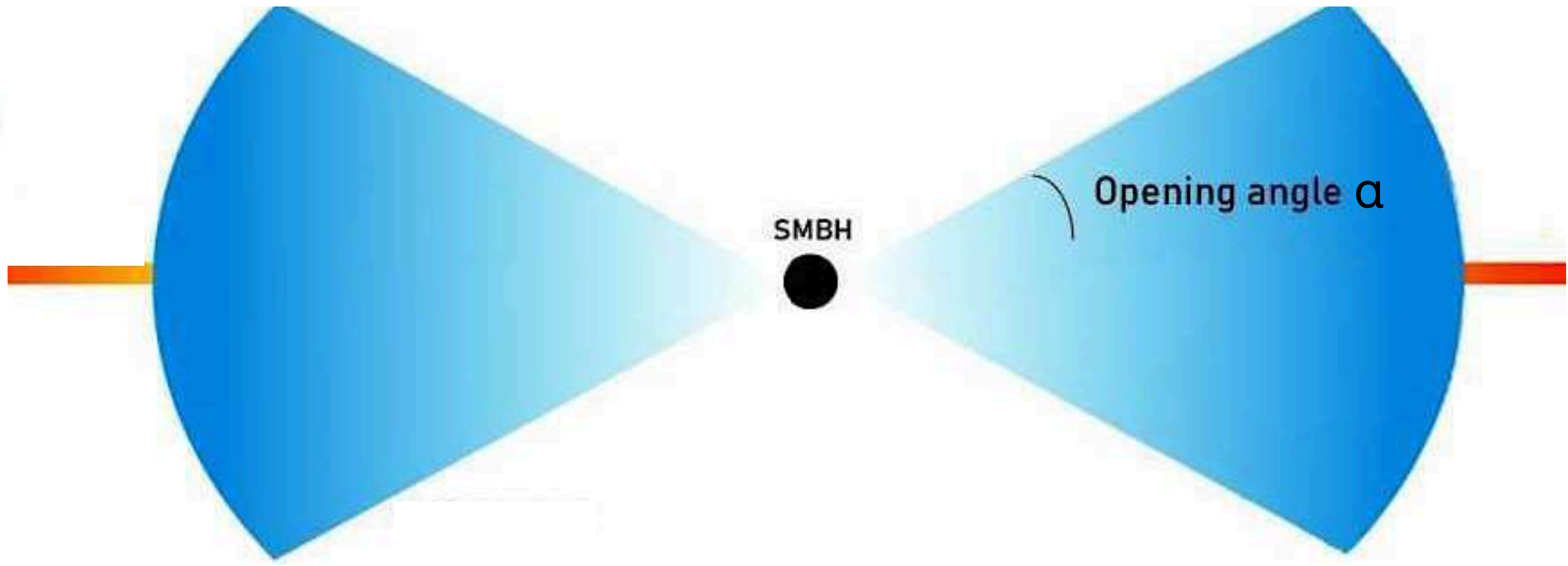

Tagliacozzo et al., subm.

Coronal geometry(ies)

For the slab and wedge geometry:

comparison with Monte Carlo radiative transfer code MONK
(Zhang et al., 2019; Ursini et al., 2022; Tagliacozzo et al., in prep)

cross-check with an iterative radiation transport solver
(Poutanen & Svensson, 1996; Veledina & Poutanen, 2022)

Coronal geometry(ies)

slab and wedge ($\alpha = 30°$): more constrained inclination 40°–70°

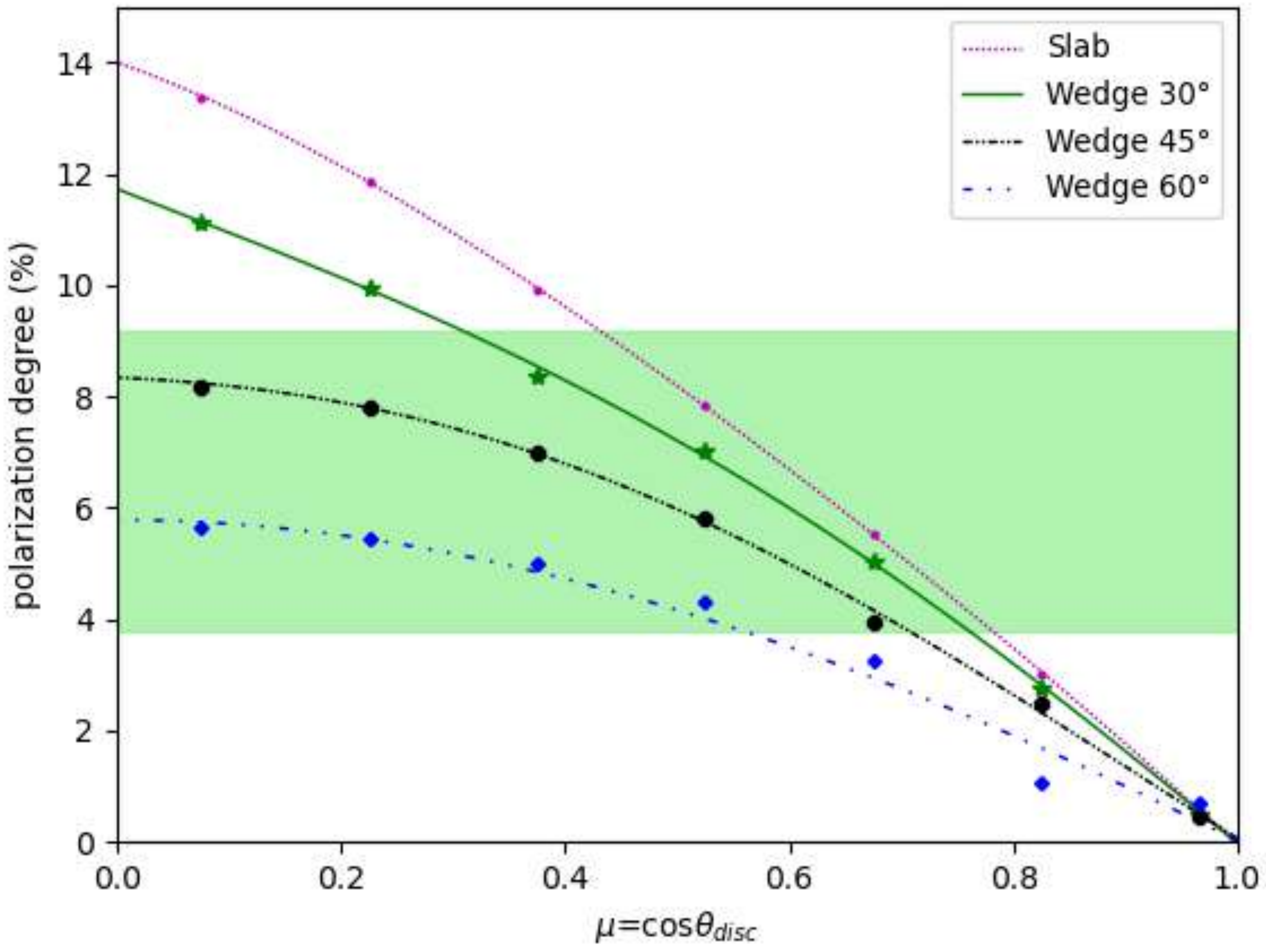

wedge ($\alpha = 45,60°$): for $\theta_{disc} > 40^{\circ}$

Conclusions

Thank you for your attention!

- polarimetric results in the 2-8 keV band → model-independent analysis (PCUBE):

$\Pi = 4.9 \pm 1.1\%$, $\Psi = 86 \pm 7°$ (1σ)

→ spectro-polarimetric analysis:

$\Pi_P = 4.3 \pm 0.8\%$, $\Psi_P = 81 \pm 7°$ (1σ) | $\Pi_P = 7.7 \pm 1.5\%$, $\Psi_P = 87 \pm 6°$ (1σ)

$\Pi_R = 20\%$ fix | $\Pi_R < 14\ \%$ (3σ)

-Ψ measured in X-ray are well aligned with the one in UV, optical, NIR and nuclear radio jet, PA ~ 83°
(Harrison et al., 1986)

- The obtained Π and Ψ exclude a 'spherical' *lamppost* geometry for the corona

- MONK and iterative radiation transport solver simulations suggest a *slab*-like or *wedge* geometry

Future: IXPE GO program…

vittoria.gianolli@univ-grenoble-alpes.fr

XMM-NuSTAR spectra

	Date	Obs ID	Exposure time	Net counts rate
XMM-A + NuSTAR-A	14/11/2012	0679780301; 60001111005	~3ks; ~62ks	~12.4cts/s; ~4.7cts/s
XMM-H	27/5/2003	143500301	12ks	~ 25.6cts/s
XMM-L	10/6/2012	679780201	~6ks	~8.6cts/s
XMM-N + NuSTAR+N	17/12/2022 16-18/12/2022	0921160201; 60901003002	~33ks; ~97ks	~ 17.2cts/s; 7.6cts/s

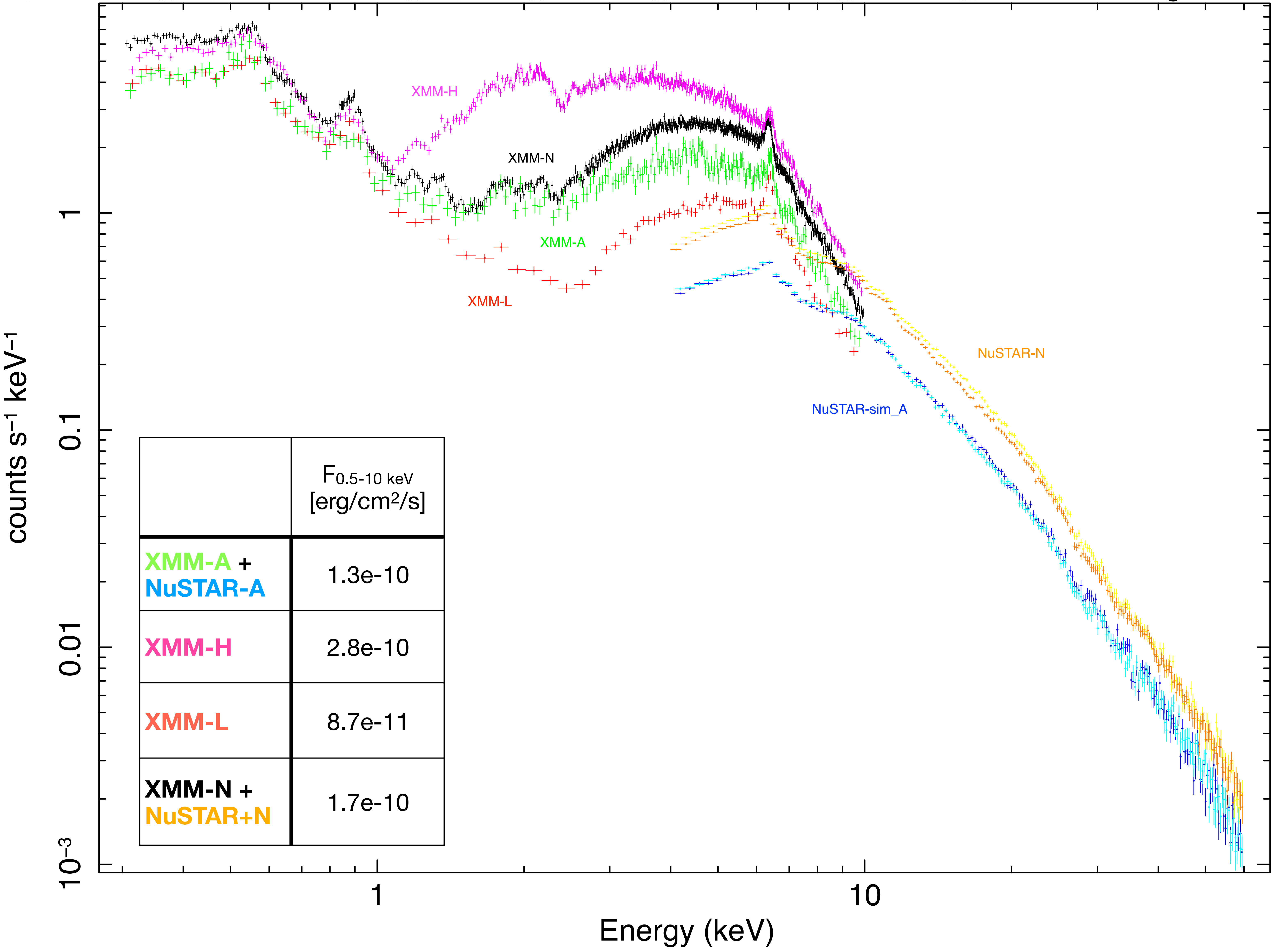

	$F_{0.5-10\ keV}$ [erg/cm²/s]
XMM-A + NuSTAR-A	1.3e-10
XMM-H	2.8e-10
XMM-L	8.7e-11
XMM-N + NuSTAR+N	1.7e-10

Polarimetric analysis

Detection significance of the polarization properties is above 99.99% confidence level ($\sim 4.4\sigma$).

Energy dependency of the polarization: hypothesis that Q and U Stokes parameters are constant via a χ^2 test

- we adopt from 2 to 12 energy bins.
- Statistically significant ($> 99\%$ c.l.) deviation from the constant behaviour in Q, when adopting three and four bins.

If 3 energy bands are considered (2.0–3.5, 3.5–5.0, and 5.0–8.0 keV):

- significant detections are found for the two higher-energy bins
- marginal detection can be claimed for the first bin

=> confirming the variability in Q mentioned above

PCUBE analysis

PCUBE is an algorithm of *ixpeobssim*, which is a simulation and analysis framework specifically developed for IXPE (Baldini et al., 2022)

It computes the I-normalized Stokes parameters Q and U from the event-by-event Stokes parameters of the selected events.

If the background template is provided, the algorithm can also calculate the background-subtracted Stokes parameters.

Following $\text{Polarization Degree} = \Pi = \frac{\sqrt{Q^2 + U^2}}{I}$, PD and PA with associated errors are calculated

$$\text{Polarization Angle} = \Psi = \frac{1}{2} arctg(\frac{U}{Q})$$

Fe Kα line

The Fe Kα line can be modeled by a single Gaussian with $\sigma = 40 \pm 10$ eV and EW = 100 ± 6 eV.

It presents a modest broadening: we convolve the BORUS tables with a gsmooth of 28^{+15}_{-17} eV.
This order of broadening is usually found in iron lines of AGN (notably in Compton-thick AGN).
And the origin of the line can be attributed to the BLR or the inner torus.

Wedge geometry

disk is truncated at radius r = 25Rg

the X-ray corona acts as a "hot accretion flow" that takes over the disk, and extends down to the ISCO.

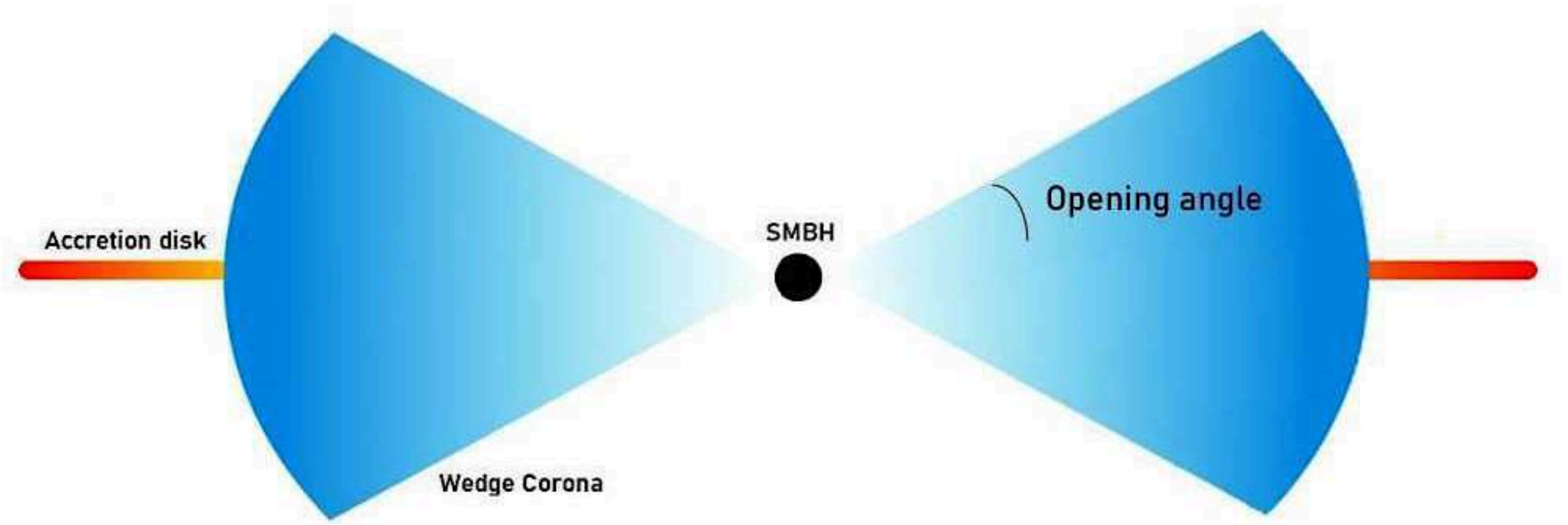

a=0.998 ?

The spin could not be constrained during the spectral analysis. However, in order to have r_{ISCO} as closer as possible to the SMBH, we opted for the maximum spin value.

In addition, in the literature it is reported that NGC 4151 should have a a>0.94 (Keck et al. 2015)

We note that, from the MONK simulations and cross-check, by considering a=0 the results do not change.

IXPE-XMM-NuSTAR: light curves

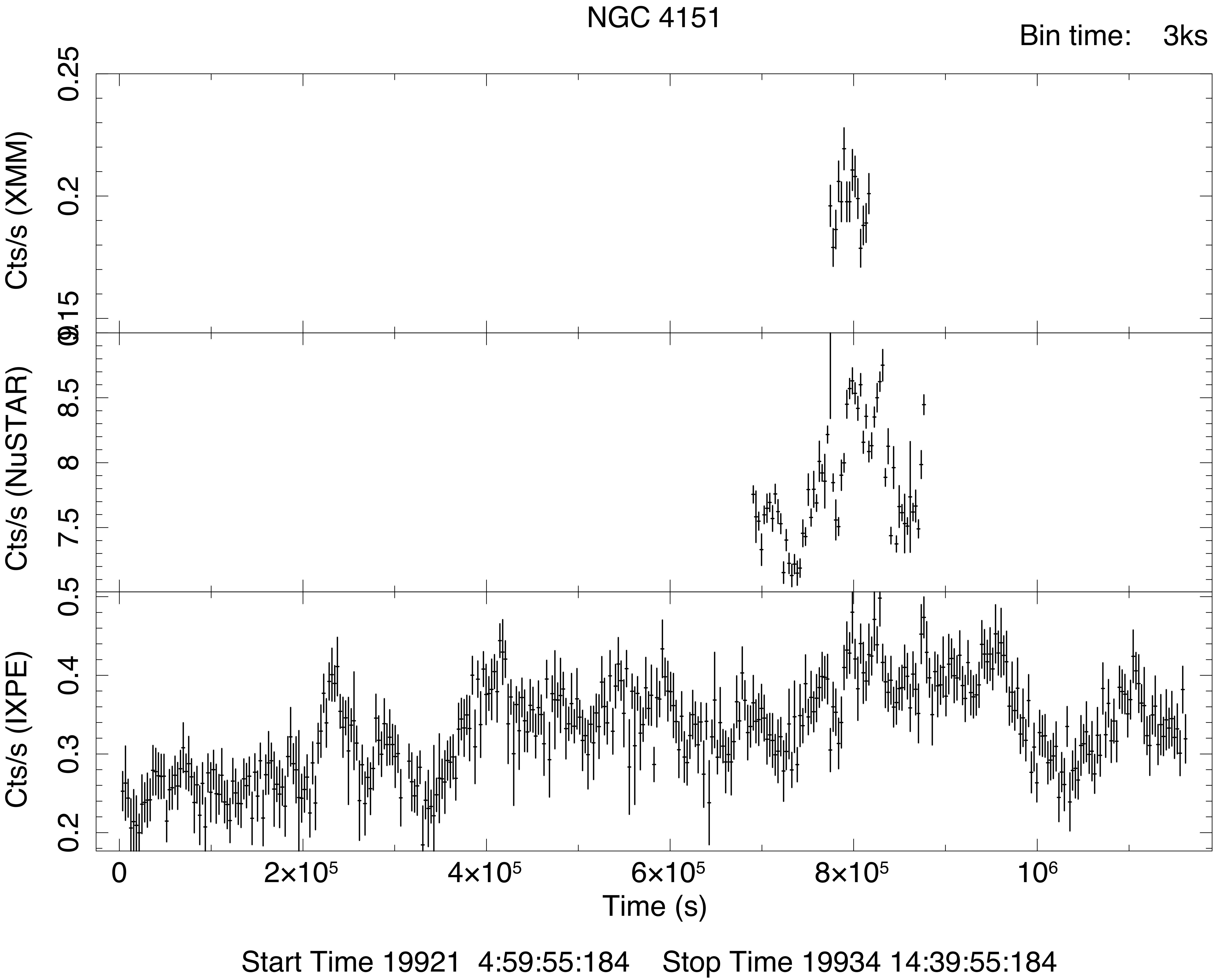

Broadband analysis

The importance of a broadband analysis:

Asses the possible contribution of the Compton reflection to the high energy end of the IXPE band.

Constrain the physical properties of the corona (kT_e,τ)

IXPE 2-8 keV

XMM-Newton 0.2-12 keV

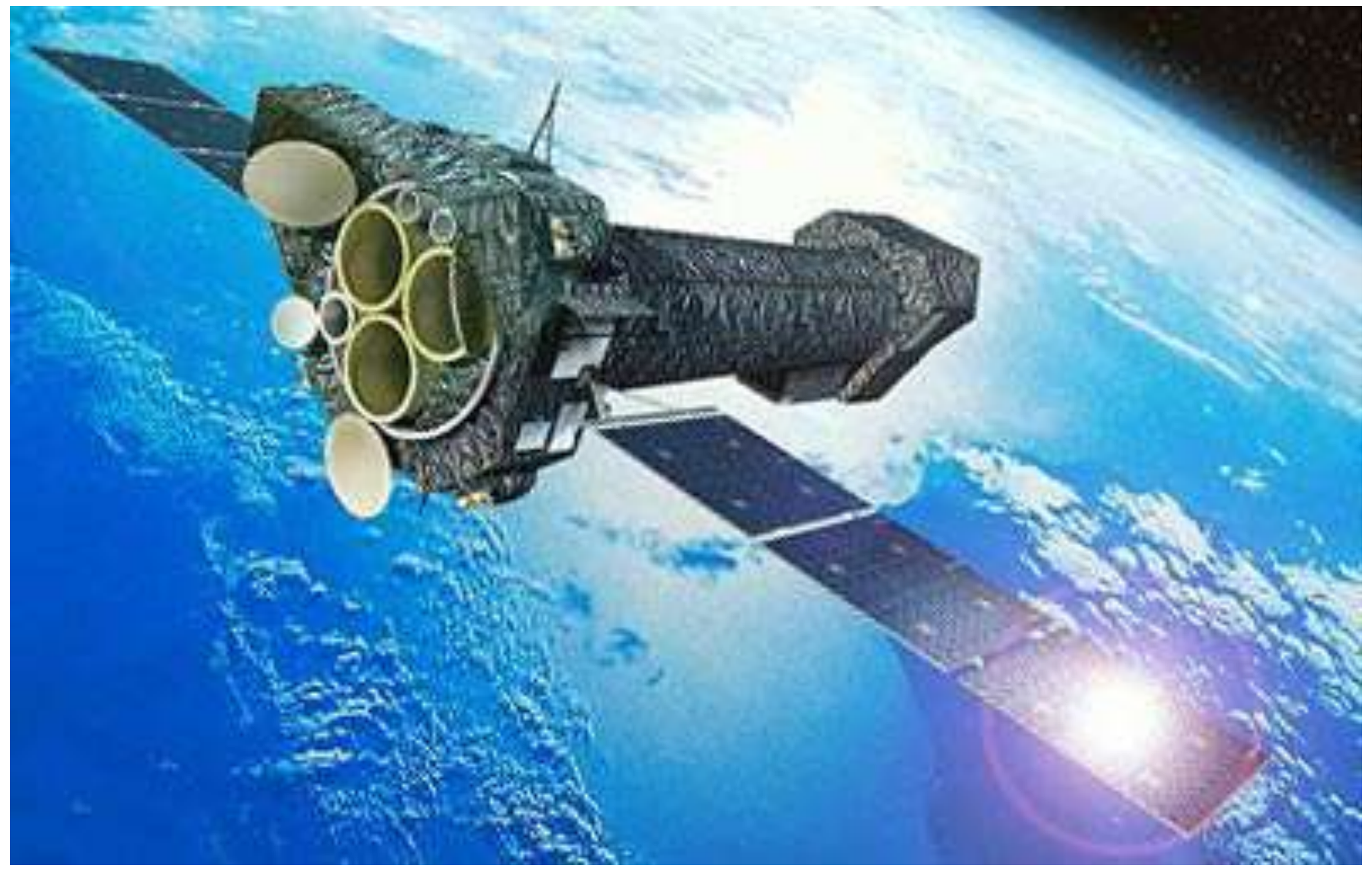

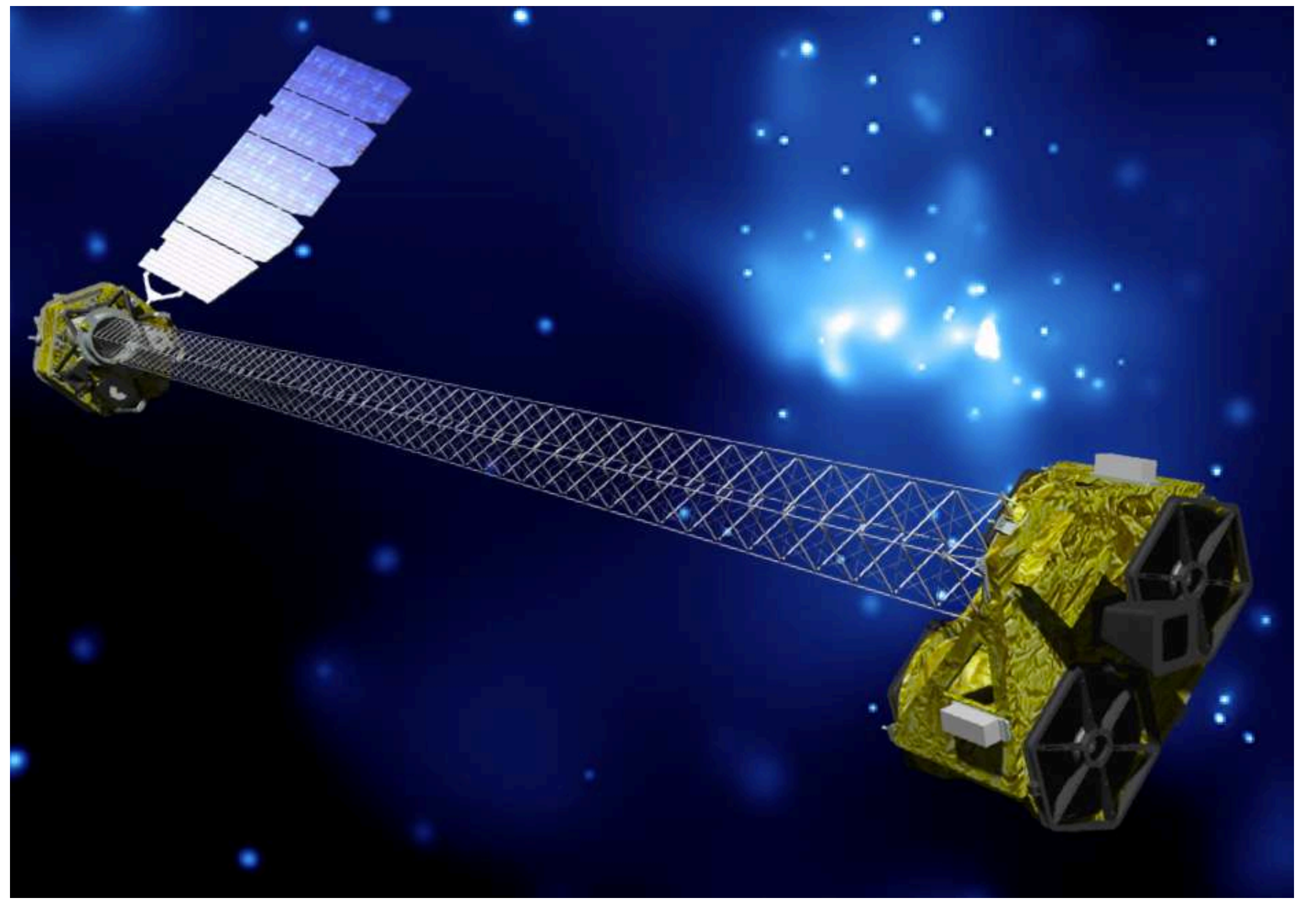

NuSTAR 3-79 keV